

High-temperature, structural disorder, phase transitions, and piezoelectric properties of GaPO₄

J. Haines,* O. Cambon, N. Prudhomme, and G. Fraysse

Laboratoire de Physico-Chimie de la Matière Condensée, UMR CNRS 5617, Université Montpellier II, Place Eugène Bataillon, cc003, 34095 Montpellier cedex 5, France

D. A. Keen

Department of Physics, Oxford University, Clarendon Laboratory, Parks Road, Oxford OX1 3PU, United Kingdom and ISIS Facility, Rutherford Appleton Laboratory, Chilton, Didcot, Oxfordshire OX11 0QX, United Kingdom

L. C. Chapon

ISIS Facility, Rutherford Appleton Laboratory, Chilton, Didcot, Oxfordshire OX11 0QX, United Kingdom

M. G. Tucker

Department of Earth Sciences, University of Cambridge, Downing Street, Cambridge CB2 3EQ, United Kingdom

(Received 15 September 2005; published 6 January 2006)

Gallium orthophosphate was studied at high temperature up to 1303 K by total neutron scattering and 1173 K by piezoelectric measurements. Rietveld refinements at 1223 K confirm the stability of the structural distortion in the α -quartz-type phase with an average tilt angle $\delta=18.8^\circ$ at this temperature. In contrast, reverse Monte Carlo (RMC) refinements of total neutron scattering data indicate that, whereas the degree of structural disorder initially slowly varies over a very large temperature interval in the α -quartz-type phase, an increase in disorder is observed beginning above 1023 K. Piezoelectric measurements indicate that the quality factor (Q) of GaPO₄ resonators remains stable up to this temperature above which the piezoelectric properties of the material degrade. This degradation can be correlated to the increase in structural disorder. RMC refinements indicate that the high-temperature β -cristobalite-type phase at 1303 K is characterized by significant thermally induced disorder with oxygen atom density forming a continuous ring around the vector joining neighboring gallium and phosphorous atoms. Gallium phosphate may be expected to retain its piezoelectric properties up to within 200 K of the phase transition temperature and as a consequence be used in applications at temperatures slightly above 1000 K.

DOI: [10.1103/PhysRevB.73.014103](https://doi.org/10.1103/PhysRevB.73.014103)

PACS number(s): 77.65.Fs, 61.12.-q, 61.43.Bn, 64.70.Kb

I. INTRODUCTION

The high-temperature behavior of silica (SiO₂) is of great interest for solid state physics, materials (piezoelectric devices, glass, vitroceraamics) and Earth sciences. Transitions are observed at high temperature from the stable phase at room temperature, trigonal α -quartz, to hexagonal β -quartz, HP(hexagonal primitive)-tridymite and finally to cubic β -cristobalite.¹ There has been considerable controversy concerning the structure and the nature of the disorder in the high-temperature forms. Recent total neutron scattering studies indicate that domain models are inappropriate to describe the disorder present in these phases.²⁻⁴ Instead, the thermally induced dynamic disorder can be related to excited rigid-unit modes (RUMs).⁵ There is, for example, no evidence for preferred oxygen sites around the ring perpendicular to the Si-Si direction in the β -cristobalite phase.² Significant disorder was also found in α -quartz prior to the α - β transition and the level of thermally induced disorder is relatively insensitive to the phase transition.⁴ The investigation of structural disorder in the high-temperature phases of silica analogs (GeO₂, AlPO₄, etc.) is much more limited⁶⁻⁸ and the results are not yet conclusive although again there is evidence for dynamic disorder,⁷ especially in the β -quartz form of AlPO₄.

The presence of dynamic disorder has a major influence on the physical properties of the different forms of silica and

its analogs. α -quartz is the most commonly used piezoelectric material, even though its performance is limited at high temperature. This has important repercussions for applications in microbalances, pressure sensors and field-test viscometers. Piezoelectric properties are limited in principle by the α - β phase transition⁹ at 846 K. In addition, our recent piezoelectric and total neutron scattering measurements show that the piezoelectric properties of α -quartz resonators, particularly the mechanical quality factor Q , degrade beginning above 573 K and can be linked to increasing structural disorder found using total neutron scattering measurements.¹⁰ Analysis of these data by reverse Monte Carlo (RMC) modeling indicated that in this temperature range the local disorder in the instantaneous structure of α -quartz becomes comparable to that of β -quartz, β -cristobalite, and silica glass. This local dynamic disorder in α -quartz at high temperature rapidly dissipates the induced dipoles and results in the observed decrease in Q .

Structure-property relationships have been developed for α -quartz and ternary α -berlinite (AlPO₄) isotypes at ambient temperature in order to identify new materials with better intrinsic properties.¹¹⁻¹⁹ The latter structure type (space group $P3_121$ or $P3_221$, $Z=3$, as for α -quartz) corresponds to a cation-ordered derivative of the α -quartz type with a doubled c parameter. The thermal stability of the α -quartz-type form and the piezoelectric response were

found to be a function of the structural distortion of a material with respect to the β -quartz structure type. This distortion in the α -quartz structure type²⁰ can be described in terms of the average intertetrahedral bridging angle θ and tetrahedral tilt angle δ . (Note that for α -quartz at room temperature, $\theta=143.6^\circ$, $\delta=16.4^\circ$ and for β -quartz at 848 K, $\theta=153.3^\circ$, $\delta=0^\circ$.²¹) The larger the tilt angle δ and the smaller the bridging angle θ the greater the distortion. One of the most promising materials identified is GaPO₄, which exhibits a high degree of structural distortion²² ($\theta=134.6^\circ$, $\delta=23.3^\circ$). The thermal stability is also high as the tilt angle δ only decreases from 23.3° at 293 K to 20.6° at 1023 K and, unlike quartz, no α - β transition is observed. Furthermore, the piezoelectric coupling coefficient of 16% is more than double that of α -quartz.¹² Due to these exceptional properties, GaPO₄ is beginning to replace α -quartz in several device applications where high temperatures are encountered.

The reconstructive transition to the β -cristobalite form of GaPO₄ only intervenes above 1206 K and is associated with very slow kinetics.²³ The structure of this form has been previously investigated by x-ray powder diffraction,^{24–27} however, only the time-averaged structure was refined. The nature and degree of thermally-induced disorder in this phase have not yet been described. Upon rapid cooling a metastable α -cristobalite form is obtained, whereas on slow cooling the reverse transition to the α -quartz-type phase is observed.^{24,25} The aim of the present study was to investigate GaPO₄ by total neutron scattering at high temperature in order to characterize the thermally induced disorder present in the material, which could result in a degradation of its piezoelectric properties, and to characterize the high-temperature, disordered, β -cristobalite-type phase.

II. EXPERIMENTAL

A. Sample preparation

GaPO₄ powder was prepared by dissolving 4N gallium metal in nitric acid followed by precipitation with phosphoric acid. The powdered sample was washed, dried and heated at 700 °C for 2 h in order to eliminate the maximum amount of hydroxyl groups.

B. Total neutron scattering

GaPO₄ was studied as a function of temperature on the GEM time-of-flight (TOF) neutron powder diffractometer²⁸ at the ISIS spallation source of the Rutherford Appleton Laboratory (RAL). 2.3 cm³ of the α -quartz type phase was placed in an 8 mm diameter cylindrical vanadium sample can in a RAL furnace equipped with a vanadium heating element. Detection was performed using six banks of ZnS scintillators: bank 1 ($6^\circ < 2\theta < 13^\circ$), bank 2 ($14^\circ < 2\theta < 21^\circ$), bank 3 ($25^\circ < 2\theta < 45^\circ$), bank 4 ($50^\circ < 2\theta < 76^\circ$), bank 5 ($79^\circ < 2\theta < 104^\circ$), bank 6 ($142^\circ < 2\theta < 149^\circ$). Data were obtained over a TOF range from 0.8 to 20 ms. Calibration runs were performed on a vanadium rod, the empty furnace, the empty can in the furnace, and the empty instrument in order to correctly account for background contributions and to normalize the data on an absolute scale. The normal-

ization procedure was carried out using the GUDRUN program, which is based on the ATLAS analysis package.²⁹ Total scattering data were acquired for approximately 3 h at each temperature to obtain the needed very good statistics, particularly in the important high- Q region, and to cover a wide range of momentum transfers for good real-space resolution. Additionally the data were normalized with respect to a standard vanadium sample and corrected for absorption for Rietveld structure refinements.

C. Structure refinements

Rietveld refinements for the α -quartz-type phase were performed using the program GSAS (Ref. 30) using the data from detector banks 3 ($d=1-5$ Å), 4 ($d=0.7-3.714$ Å), 5 ($d=0.5-2.385$ Å), and 6 ($d=0.5-1.765$ Å). The cell constants, atomic positions, anisotropic atomic displacement parameters, scale factor and two line shape parameters were varied in the refinements, along with up to 30 background parameters to account for background contributions due to diffuse scattering. The anisotropic atomic displacement parameters of the two crystallographically independent oxygen atoms were constrained to be identical for temperatures between 923 and 1223 K. Soft restraints were applied to the P-O distances (1.52 Å) for data obtained in this temperature range. In the absence of such constraints a significant dispersion in the P-O distances was observed, however, the average distance was not greatly affected. Similar refinements were carried out on data from the cristobalite phases.

D. Pair distribution functions

The neutron weighted, total pair distribution functions $G(r)$ are the sine Fourier transform of the neutron total scattering structure factors $F(Q)$. In this case, normalized total scattering data from different GEM detector banks are merged together to form one $F(Q)$ for each temperature over as wide a range of Q as possible. These composite $F(Q)$ are then Fourier transformed to $G(r)$ using the following function:

$$G(r) = \frac{1}{(2\pi)^3 \rho_0} \int_0^\infty 4\pi Q^2 F(Q) \frac{\sin(Qr)}{Qr} dQ, \quad (1)$$

where ρ_0 is the number density of the material and $G(r)$ is a neutron weighted summation of the $\frac{1}{2}n(n+1)$ partial radial distribution functions $g_{ij}(r)$ given by

$$G(r) = \sum_{i,j=1}^n c_i c_j \bar{b}_i \bar{b}_j [g_{ij}(r) - 1], \quad (2)$$

where n is the number of atom species in the material and c_i and \bar{b}_i are the proportion and neutron-scattering length of species i , respectively. The $g_{ij}(r)$ functions contain information about the number of atoms of type i around an atom of type j , averaged over all j atoms. They relate to the instantaneous structure (i.e., a “snap-shot”) and as such give complementary structural information to the “average” structure determined from Rietveld analysis of Bragg intensities.

TABLE I. Unit cell parameters, volume, and agreement factors for trigonal, α -quartz-type GaPO₄ as a function of temperature.

T (K)	a (Å)	c (Å)	V (Å ³)	R_{wp}	R_p	χ^2
306	4.89606(2)	11.02565(7)	228.890(2)	0.029	0.031	8.3
473	4.90701(2)	11.0353(1)	230.117(2)	0.029	0.031	7.4
673	4.92174(2)	11.0495(1)	231.797(2)	0.029	0.031	6.7
873	4.93857(2)	11.0661(1)	233.737(2)	0.029	0.031	6.2
923	4.94464(3)	11.0675(1)	234.342(2)	0.039	0.033	10.8
973	4.94826(2)	11.0755(1)	234.854(2)	0.029	0.031	5.8
1023	4.95426(3)	11.0783(1)	235.484(2)	0.041	0.034	11.0
1073	4.95921(3)	11.0841(1)	236.079(2)	0.034	0.031	7.7
1123	4.96526(4)	11.0894(1)	236.768(3)	0.045	0.035	12.6
1173	4.97184(4)	11.0939(1)	237.492(3)	0.045	0.034	12.1
1223	4.97897(2)	11.0981(1)	238.264(2)	0.027	0.027	3.4

Note that different formalisms exist for describing these functions and a summary of their inter-relationships may be found in Ref. 31. The differential correlation function $D(r)$ in particular is also used in the present work and is obtained from $G(r)$ as follows:

$$D(r) = 4\pi r \rho_0 G(r). \quad (3)$$

E. RMC modeling

The general principles of RMC modeling and how it may be applied to crystalline materials have been reviewed in detail in Refs. 32 and 33, respectively. Briefly, a supercell of the average crystalline unit cell is created and randomly chosen atoms within this supercell are moved one at a time a random amount. Each time a move is attempted various structural functions are calculated and compared with the equivalent experimental data. If the agreement improves then the move is accepted and if the agreement worsens then the move is accepted with a reduced probability. The process is continued until the agreement function χ_{RMC}^2 is minimized

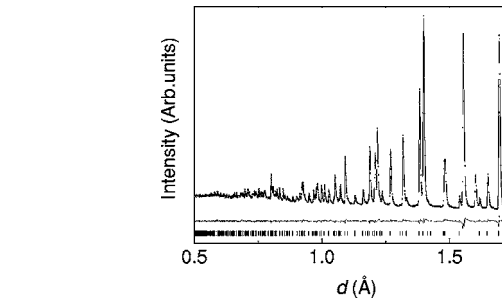


FIG. 1. Experimental and calculated profiles from the Rietveld refinement of trigonal, α -quartz-type GaPO₄ at 873 K. Data from the GEM detector bank 6 ($142^\circ < 2\theta < 149^\circ$) are shown. The difference profile is on the same scale. Vertical ticks indicate the calculated positions of the reflections.

and further moves cause χ_{RMC}^2 to fluctuate about this minimum value. Here, χ_{RMC}^2 is defined as

$$\chi_{\text{RMC}}^2 = \chi_{\text{data}}^2 + \chi_{\text{restraints}}^2, \quad (4)$$

where

$$\begin{aligned} \chi_{\text{data}}^2 = & \sum_n [F_{\text{calc}}(Q_i) - F_{\text{exp}}(Q_i)]^2 / \sigma_{F(Q)}(Q_i) \\ & + \sum_m [D_{\text{calc}}(r_i) - D_{\text{exp}}(r_i)]^2 / \sigma_{D(r)}(r_i) \\ & + \sum_l [I_{\text{calc}}(t_i) - I_{\text{exp}}(t_i)]^2 / \sigma_{I(t)}(t_i) \end{aligned} \quad (5)$$

summing over the n , m , and l points of $F(Q)$, $D(r)$ and $I(t)$, respectively. $D(r)$ is related to $G(r)$ defined above (see Ref. 31) and $I(t)$ is the powder profile. $\chi_{\text{restraints}}^2$ is defined as

$$\begin{aligned} \chi_{\text{restraints}}^2 = & w_{A-O} \sum_{A-O} (r_{A-O} - R_{A-O})^2 \\ & + w_{O-A-O} \sum_{O-A-O} (\theta_{O-A-O} - \Theta_{O-A-O})^2 \end{aligned} \quad (6)$$

summing over all the intratetrahedral A-O bond lengths and

TABLE II. Fractional atomic coordinates and equivalent isotropic atomic displacement parameters (Å²) for α -quartz-type GaPO₄. P3₁21-Ga on 3a ($x, 0, 1/3$), P on 3b ($x, 0, 5/6$), O1, O2 on 6c (x, y, z).

T (K)	$x_{(\text{Al,Ga})}$	100^*U_{eq}	x_P	100^*U_{eq}	x_{O1}	y_{O1}	z_{O1}	100^*U_{eq}	x_{O2}	y_{O2}	z_{O2}	100^*U_{eq}
306	0.4557(2)	0.48(4)	0.4562(2)	0.60(6)	0.4103(2)	0.3185(2)	0.3925(1)	1.00(4)	0.4080(2)	0.2717(2)	0.8724(1)	1.03(4)
473	0.4568(2)	0.84(5)	0.4580(3)	0.93(7)	0.4104(2)	0.3160(2)	0.3932(1)	1.62(5)	0.4094(3)	0.2699(2)	0.8731(1)	1.70(5)
673	0.4584(2)	1.27(7)	0.4598(3)	1.38(9)	0.4108(3)	0.3129(2)	0.3939(1)	2.40(6)	0.4112(3)	0.2672(2)	0.8742(1)	2.55(7)
873	0.4598(3)	1.77(8)	0.4622(4)	1.82(11)	0.4115(3)	0.3094(3)	0.3949(1)	3.41(8)	0.4130(4)	0.2643(3)	0.8756(1)	3.49(8)
923	0.4615(3)	1.86(11)	0.4602(4)	2.22(16)	0.4095(4)	0.3052(3)	0.3955(1)	3.75(6)	0.4161(4)	0.2663(4)	0.8764(1)	3.75(6)
973	0.4608(2)	2.03(9)	0.4640(3)	2.09(12)	0.4118(3)	0.3068(3)	0.3958(1)	4.01(5)	0.4140(4)	0.2630(3)	0.8762(1)	4.01(5)
1023	0.4630(3)	2.06(12)	0.4611(4)	2.67(18)	0.4098(4)	0.3023(4)	0.3964(1)	4.33(7)	0.4179(5)	0.2655(4)	0.8772(1)	4.33(7)
1073	0.4634(3)	2.25(11)	0.4629(4)	2.74(17)	0.4106(4)	0.3012(3)	0.3969(1)	4.60(6)	0.4176(4)	0.2638(4)	0.8776(1)	4.60(6)
1123	0.4641(4)	2.30(14)	0.4623(5)	3.12(22)	0.4105(5)	0.2989(4)	0.3973(1)	4.99(8)	0.4197(6)	0.2645(5)	0.8783(2)	4.99(8)
1173	0.4650(4)	2.37(14)	0.4636(5)	3.41(23)	0.4103(5)	0.2966(4)	0.3979(1)	5.36(9)	0.4200(6)	0.2633(5)	0.8790(2)	5.36(9)
1223	0.4655(3)	2.69(9)	0.4677(3)	3.00(14)	0.4137(4)	0.2999(3)	0.3980(1)	5.64(5)	0.4157(4)	0.2561(3)	0.8798(1)	5.64(5)

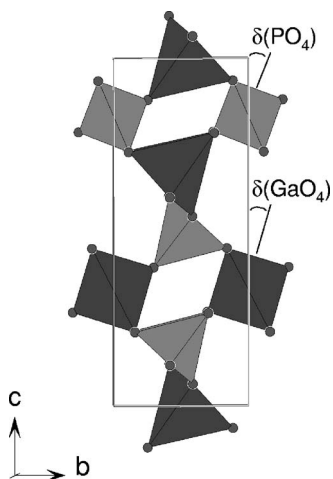


FIG. 2. Polyhedral representation of the crystal structure of GaPO₄ at 1223 K viewed along the *a* direction. Polyhedra containing Ga are shaded dark gray; those containing P are shaded light gray. The angle δ corresponds to the tilt of the tetrahedra about their twofold axes parallel to *a* with respect to their orientation in the β -quartz-type structure (i.e., with projected A-O and B-O bond vectors at $\pm 45^\circ$).

O-A-O bond angles ($A=\text{Ga},\text{P}$) within the supercell, respectively. $R_{\text{P-O}}$ and $R_{\text{Ga-O}}$ were determined from the two lowest- r peaks in $G(r)$, respectively, and $\Theta_{\text{O-P-O}}$ and $\Theta_{\text{O-Ga-O}}$ were both set to the ideal tetrahedral angle (109.47°). A low weighting, w , on each restraint was applied to ensure that the low- r peaks in $G(r)$ were not sharper than those observed experimentally, and to allow the distributions of distances and angles to reflect the experimental data rather than the restraint. These restraints also ensured that the topology of the network structure was preserved during RMC minimization.

F. Piezoelectric measurements

The piezoelectric response of the resonators was measured using a Hewlett-Packard 8753A network analyzer.

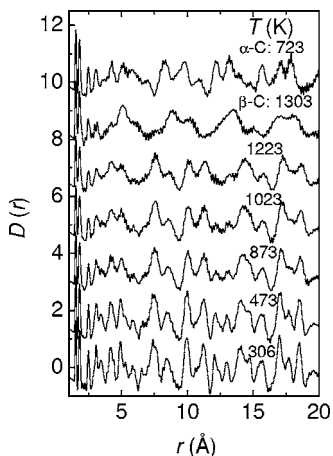


FIG. 3. Neutron pair distribution functions for GaPO₄ as a function of temperature ($\alpha\text{-C}=\alpha$ -cristobalite, $\beta\text{-C}=\beta$ -cristobalite).

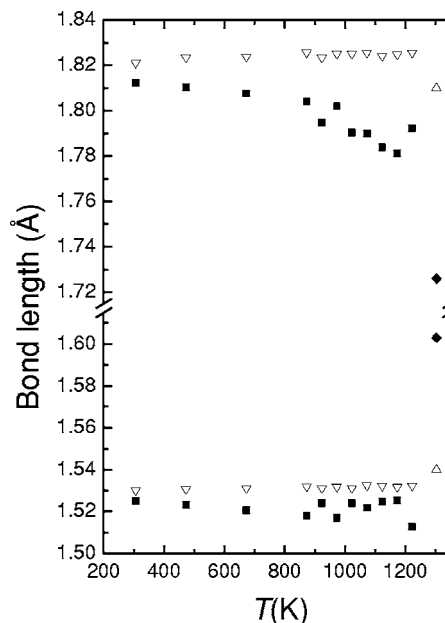


FIG. 4. Ga-O and P-O bond lengths as a function of temperature obtained by Rietveld refinement ($\blacksquare, \blacklozenge$) and by total neutron scattering (∇, \triangle). The values given for 1303 K correspond to the β -cristobalite-type phase.

High-temperature experiments were performed in a controlled temperature furnace ($\pm 0.5^\circ\text{C}$). GaPO₄ resonators (Piezocryst GMBH) were based on AT-cut (-15.9° Y-rotated cut) plates using the fundamental thickness shear mode. The metallized plate was maintained with two conductive metallic clips on the electrodes ensuring the electrical excitation of the resonator.

III. RESULTS AND DISCUSSION

A. Stability of the α -quartz-type structure

1. Rietveld refinements—average structure

Rietveld refinements (Tables I and II, Fig. 1) confirmed the stability of the α -quartz-type form of GaPO₄ from

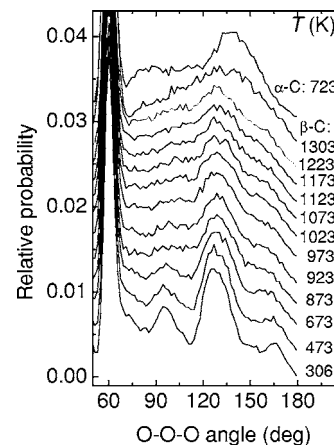


FIG. 5. Distribution functions of the intertetrahedral O-O-O angle in GaPO₄ as a function of temperature ($\alpha\text{-C}=\alpha$ -cristobalite, $\beta\text{-C}=\beta$ -cristobalite). Intratetrahedral O-O-O angles form the peak centered at 60° (offscale).

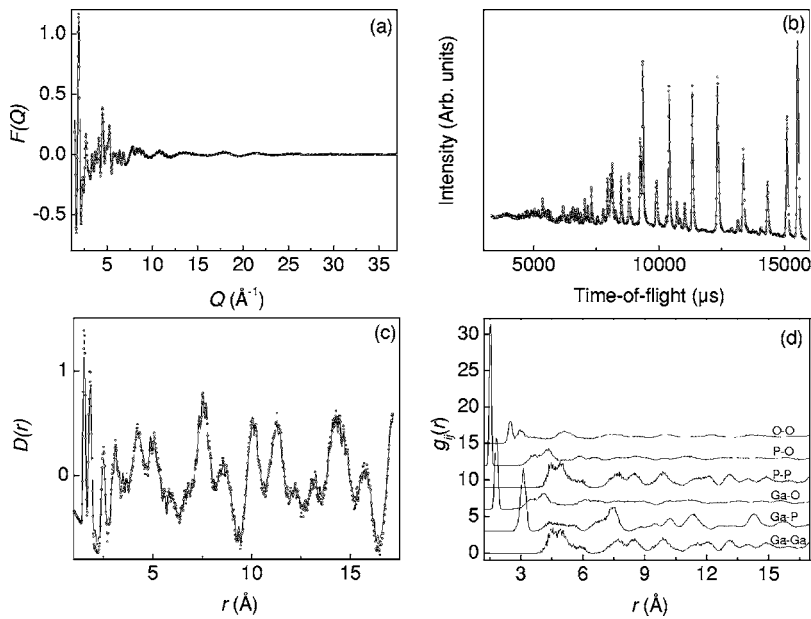


FIG. 6. Experimental and calculated profiles from the reverse Monte Carlo refinement of the (a) neutron total scattering structure factor, (b) neutron powder diffraction data and (c) neutron differential correlation function data for α -quartz-type GaPO_4 at 1223 K. Partial radial distribution functions are shown in (d).

306 to 1223 K (Fig. 2). The thermal expansion coefficient ($T \geq 306$ K) can be expressed as follows: $\alpha_T(\text{K}^{-1}) = 3.29 \times 10^{-5} + 2.766 \times 10^{-11}(T-306)^2$. The room temperature value is similar to that of α -quartz-type FePO_4 ($2.924 \times 10^{-5} \text{ K}^{-1}$)³⁴ and lower than those of α -quartz ($3.7 \times 10^{-5} \text{ K}^{-1}$)³⁵ and AlPO_4 ($3.97 \times 10^{-5} \text{ K}^{-1}$).³⁶ The structural data are in good agreement with previous single-crystal^{22,37-39} and powder^{40,41} x-ray diffraction studies. In the present study, data are obtained up to higher temperatures and the use of neutrons provides more accurate fractional coordinates for the light oxygen atoms. The expected increase of the Ga-O and P-O bond lengths as a function of temperature in the time-averaged structure is not observed. This is similar to the results obtained for the average structures of many other α -quartz homeotypes and can be related to thermally induced disorder (see Sec. III A 2 below). This effect is most marked for the least-distorted (SiO_2 and AlPO_4) (Refs. 4 and 36) and is only minor for the most

distorted materials (GeO_2 and GaAsO_4).^{13,15,19} A more complete structural model is thus required to understand the high-temperature behavior of GaPO_4 , especially if one wants to correlate the physical properties of this material to its structure.

2. Total neutron scattering—instantaneous structure

Bondlengths may be determined directly from pair distribution functions $G(r)$ (Fig. 3), obtained from neutron total scattering structure factors $F(Q)$. The instantaneous bondlengths extracted from the pair distribution functions $G(r)$ exhibit the expected increase as a function of temperature (Fig. 4). The increasing difference between the time av-

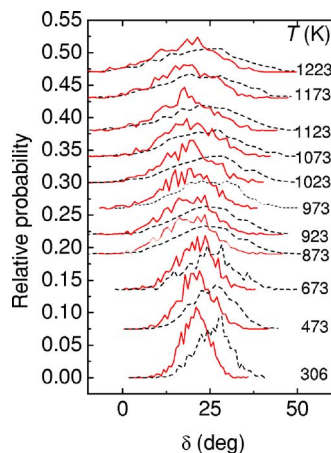


FIG. 7. (Color online) Distribution functions of the tetrahedral tilt angles $\delta(\text{GaO}_4)$ (solid line) and $\delta(\text{PO}_4)$ (dashed line) in GaPO_4 as a function of temperature.

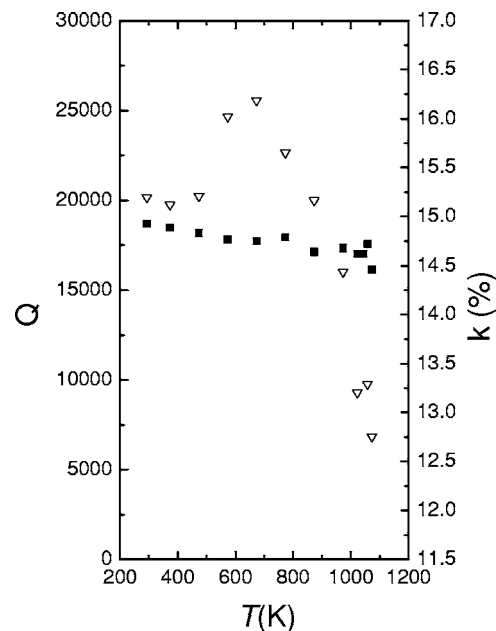


FIG. 8. Quality factor Q (∇) and piezoelectric coupling constant k (\blacksquare) of an AT-cut GaPO_4 resonator as a function of temperature.

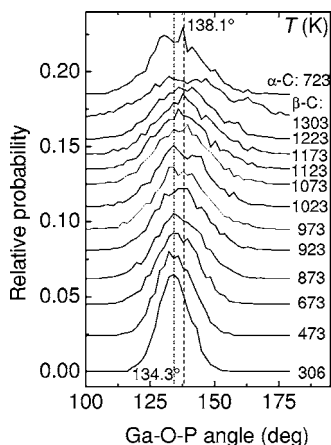


FIG. 9. Distribution functions of the intertetrahedral Ga-O-P bridging angle in GaPO₄ as a function of temperature (α -C = α -cristobalite, β -C = β -cristobalite). The extreme values for the α -quartz form are indicated by dashed lines.

eraged and instantaneous bond lengths is an indication of thermally induced disorder as observed previously for silica polymorphs at high temperature.²⁻⁴ This disorder is related to the excitation of large amplitude rigid-unit modes in these framework structures. This can clearly be seen in the pair distribution functions for values (i.e., 3–9 Å) greater than the intratetrahedral O-O distances (Fig. 3) and less than the distances which reflect the lattice repeat and in the intertetrahedral O-O-O angle distributions (Fig. 5) which represent the relative orientations of neighboring tetrahedra. These angular distributions are obtained from RMC refinement of the total scattering data (Fig. 6). A significant increase in the degree of disorder is apparent in the O-O-O angle distributions in the 973–1223 K temperature range prior to the transition to the β -cristobalite form. In contrast, there is a continuous and gradual increase in the width of the tilt angle distributions (Fig. 7) with the width at 1023 K being 2.3 times that at 306 K. The average values obtained from these distributions are in good agreement with the results of the Rietveld refinements. The relative width of the $\delta(\text{PO}_4)$ with respect to the $\delta(\text{GaO}_4)$ distributions increases only very

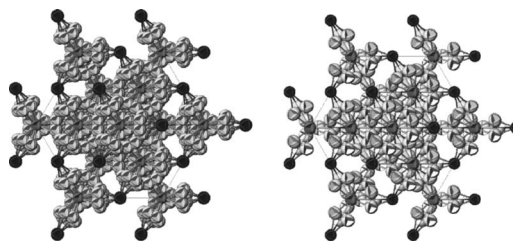


FIG. 10. The two average structures of the β -cristobalite phase of GaPO₄ at 1303 K, looking down a 111 axis. The left- and right-hand plots show the 96(*i*) and 48(*h*) model, respectively.

slightly from 1.27 to 1.32 over this temperature interval with the lighter P-centered tetrahedra always exhibiting broader distributions. This may be a sign that there is no great change in the relative degree of motion of the two different types of tetrahedra. The average δ values for the GaO₄ and PO₄ tetrahedra decrease respectively from 20.9° and 25.7° at 306 K to 16.8 and 20.8° at 1223 K indicating the relative stability of the α -quartz form. This is very different from the behavior of α -quartz (Ref. 4 and 21) (SiO₂) for which the δ value decreases strongly and then drops to 0° at the α - β phase transition at 846 K.

B. Piezoelectric results at high temperature

Piezoelectric measurements were performed on a GaPO₄ resonator up to 1073 K, the results of which are shown in Fig. 8. The piezoelectric properties of a resonator can be characterized in terms of two quantities, the mechanical quality factor Q , which is a measure of the quality of the resonator with respect to acoustic attenuation, and the electromechanical coupling coefficient k . These two properties are defined as follows:

$$Q = 2\pi L f_r / R, \quad (7)$$

$$k = \pi/2 [(f_a - f_r)/f_a]^{1/2}, \quad (8)$$

where L is the self-inductance and R is the resistance of the resonator. f_r and f_a are the frequencies of resonance and

TABLE III. Rietveld refined structural parameters for the two possible models of the β -cristobalite phase of GaPO₄ at 1303 K. (Space group $F\bar{4}3m$, cell parameter, $a=7.14520(6)$ Å, volume/formula unit $V/Z=91.197$ Å³.)

48(<i>h</i>) model		$(\chi^2=4.03)$	96(<i>i</i>) model		$(\chi^2=4.06)$
Atom	Fractional coordinates	100U (Å ²)	Fractional coordinates	100U (Å ²)	
Ga	4(<i>a</i>) (000)	$U_{\text{iso}}=8.72(11)$	4(<i>a</i>) (000)	$U_{\text{iso}}=7.04(9)$	
P	4(<i>c</i>) ($\frac{1}{4}\frac{1}{4}\frac{1}{4}$)	$U_{\text{iso}}=7.47(11)$	4(<i>c</i>) ($\frac{1}{4}\frac{1}{4}\frac{1}{4}$)	$U_{\text{iso}}=9.02(13)$	
O	48(<i>h</i>) (<i>x</i> , <i>x</i> , <i>z</i>)	$U_{11}=U_{22}=10.58(18)$	96(<i>i</i>) (<i>x</i> , <i>y</i> , <i>z</i>)	$U_{\text{iso}}=9.25(9)$	
	$x=0.0962(3)$	$U_{33}=9.58(15)$	$x=0.0708(6)$		
	$z=0.1983(4)$	$U_{12}=-0.70(20)$	$y=0.1280(9)$		
	occ=1/3	$U_{13}=U_{23}=-0.91(8)$	$z=0.1923(5)$		
			occ=1/6		

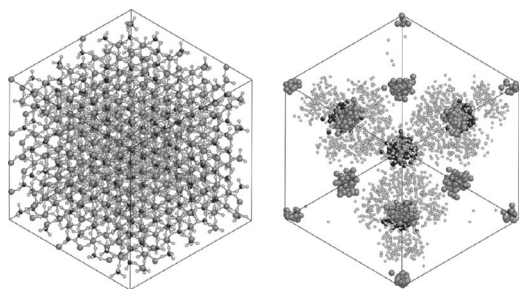


FIG. 11. RMC model of the β -cristobalite phase of GaPO_4 at 1303 K, projected down 111. The left-hand plot shows the whole configuration whereas the right-hand plot shows the atoms superimposed onto a single unit cell. Ga, P, and O atoms are large mid-gray, nearly black, and small light gray/shaded white spheres, respectively.

antiresonance, respectively. The mechanical quality factor is very sensitive to structural disorder and defects in the material and characterizes the purity of the spectral signal. In α -quartz homeotypes,^{12,13,19} the electromechanical coupling coefficient k has been correlated to the structural distortion expressed by the intertetrahedral bridging angle θ .

A high Q factor was measured up to 973 K (Fig. 8). Above this temperature, the Q value was found to decrease. This decrease continued to higher temperatures with the signal obtained at 1123 K being characteristic of a poor resonator. No signal was obtained at 1173 K. The observed decrease in Q can be correlated to the increase in structural disorder, which is particularly evident in the O-O-O angle distributions (Fig. 5). At moderate temperatures, distinct maxima are observed in the distributions. Beginning close to 973 K, the distribution widens and becomes very broad above 1123 K. This is evidence that the relative orientations of the individual tetrahedra and the corresponding dipoles are no longer correlated on a short time scale, thereby providing a mechanism for the loss of the piezoelectric signal at these temperatures. It can be noted that the tetrahedra themselves remain relatively undistorted as can be seen from the relatively unchanged Ga-O and P-O bond length and intratetrahedral O-O-O angle distributions. This further supports the model of large amplitude rigid unit vibrations as the origin of the observed disorder.

In contrast to the Q factor, the electromechanical coupling coefficient k only decreases from 14.9 to 14.5% over the temperature interval from 293 to 1073 K (Fig 8). In parallel,

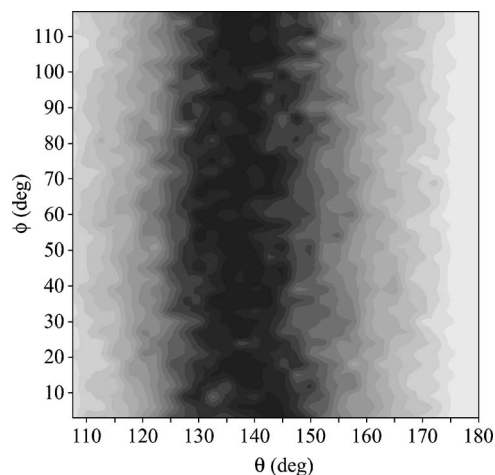


FIG. 12. Orientation of PO_4 tetrahedra about GaO_4 tetrahedra in terms of Ga-O-P bond angle θ and torsional angle ϕ .

the instantaneous average Ga-O-P angle (θ) increases from 134.3° to 137.2° , Fig. 9. Such a decrease is expected based on correlations between k and θ at ambient temperature. Note that the Rietveld refinements of the average structure overestimate the structural distortion at high temperature and thus cannot be used to establish *in situ* structure-property relationships at high temperature. The θ value obtained from Rietveld refinements, for example, increases from 134.4° at 306 K to 139.5° at 1073 K. This large increase in θ , which is almost twice that observed in the instantaneous structure, arises from the fact that the average structural model cannot accurately represent the structure when substantial disorder is present.

C. Structures of the cristobalite-type phases

The structure of the β -cristobalite phase of GaPO_4 has been investigated at 1303 K and of the α -cristobalite phase at room temperature and 723 K, using both Rietveld and RMC analysis of the neutron diffraction data. Of particular interest is the nature of the disorder apparent in the high-temperature β phase. There have been a small number of reports of this structure based on high-temperature x-ray diffraction, both for GaPO_4 (Ref. 27) and AlPO_4 (Refs. 42 and 43) (where the β -cristobalite phase occurs at lower temperatures). The structural topology of the β -cristobalite phase of both SiO_2 and GaPO_4 is the same. However, the alternation

TABLE IV. A summary of the intratetrahedral bond lengths and intertetrahedral bond angles from the cristobalite phases of GaPO_4 . (The room-temperature data were measured for too short a time to obtain meaningful total scattering data.)

	Ga-O _{Rietveld} (Å)	Ga-O _{G(r)} (Å)	P-O _{Rietveld} (Å)	P-O _{G(r)} (Å)	Ga-O-P _{Rietveld} (deg)	Ga-O-P _{RMC} (deg)
RT (α)	1.811(1)		1.522(1)		132.94(5)	
	1.812(1)		1.523(1)		135.43(5)	
723 K (α)	1.784(2)	1.81	1.509(2)	1.53	136.2(1)	135
	1.796(2)		1.522(3)		138.4(1)	
1303 K (β)	1.726(4)	1.81	1.603(3)	1.54	136.65(8)	139

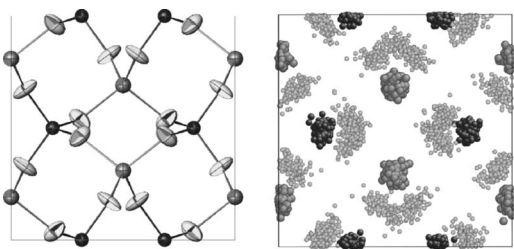


FIG. 13. The average α -cristobalite structure of GaPO_4 at 723 K obtained by Rietveld refinement (LH panel) and from the RMC model (RH panel). The unit cell is shown projected down the c axis.

of Ga and P in the tetrahedral sites reduces the $Fd\bar{3}m$ symmetry of SiO_2 (Ref. 44) to $F\bar{4}3m$ in GaPO_4 . Furthermore, it was found that the optimum position for the oxygen atoms was on the $48(h)$ (x, x, z) sites with $x=0.106(2)$ and $z=0.207(5)$, each 1/3 occupied (at 973 K).²⁷ This leads to a somewhat different picture of the thermal disorder than that of the β -cristobalite phase of SiO_2 , where the structure is characterized by a six-fold splitting of the oxygen site in $\langle 110 \rangle$ directions away from the position which is midway between the silicon atoms.⁴⁴ The low-temperature α -cristobalite phase is more ordered and is described in the orthorhombic space group $C222_1$ (see, for example, Refs. 45 or 27).

1. β -cristobalite-type structure

Various models of the oxygen disorder were attempted within space group $F\bar{4}3m$, all with Ga atoms placed on $4(a)$ (000) sites and P atoms on $4(c)$ ($\frac{1}{4}\frac{1}{4}\frac{1}{4}$) sites and no restraints on any bond lengths or angles. Of these, two yield an almost

identical, excellent fit to the diffraction data. The first, following earlier work,²⁷ placed O atoms on $48(h)$ (x, x, z) sites with anisotropic atomic displacement parameters (ADP's) and each site 1/3rd occupied. The second, considered 1/6th occupation of $96(i)$ (x, y, z) sites and isotropic ADP's. The structural parameters from both refinements are summarized in Table III. Earlier refinements of the $96(i)$ model found that it converged to the $48(h)$ model;⁴³ this minimum was also observed here, but with a slightly worse fit to the one shown in Table III [where the partially occupied O sites are 0.58(1) or 0.65(1) Å apart]. It is difficult to distinguish between the two models, since both are essentially using split-sites and ADP's to characterize thermal disorder. Figure 10 shows this clearly; although the $48(h)$ model contains fewer sites than the $96(i)$ model, anisotropic ADP's spread the atomic density in directions to encompass the $96(i)$ sites.

Inspection of the bond lengths and angles also shows little difference between the models, with values for the P-O, Ga-O bond lengths and Ga-O-P bond angles of 1.597(3) Å, [1.603(3) Å], 1.719(2) Å [1.726(4) Å], and 137.83(18)°, [136.65(8)°] respectively, for the $48(h)$ [$96(i)$] models. The $96(i)$ model produces less distorted tetrahedra, although again the difference is marginal. (For comparison, the two lowest- r peaks in the radial distribution function $G(r)$ give instantaneous bond lengths of 1.54 and 1.81 Å for P-O and Ga-O, respectively, see Table IV).

Average structural models similar to the ones above have been used in the past to suggest that the high-temperature β -cristobalite phase of SiO_2 is composed of a superposition of domains of lower symmetry.⁴⁶ However, before using these models to infer threefold or sixfold domain superpositions, it is important to consider the local structural correlations using RMC modeling (and following Ref. 44). A

TABLE V. Rietveld refined structural parameters for the α -cristobalite phase of GaPO_4 at room temperature and 723 K.

T(K) 293									
	a (Å)	b (Å)	c (Å)	V/Z (Å ³)					
	6.9716(1)	6.94840(9)	6.86967(5)	83.19					
	x	y	z	U_{iso} or U_{11} (100 Å ²)	U_{22} (100 Å ²)	U_{33} (100 Å ²)	U_{12} (100 Å ²)	U_{13} (100 Å ²)	U_{23} (100 Å ²)
Ga	0	0.1844(2)	$\frac{1}{4}$	0.71(2)					
P	0.3187(2)	0	0	0.79(3)					
O1	0.1976(1)	0.0291(1)	0.1821(1)	1.41(4)	1.65(5)	1.21(4)	0.64(3)	0.56(3)	0.33(4)
O2	0.4444(1)	0.1758(1)	0.9653(1)	1.89(4)	1.48(4)	1.04(4)	-0.99(4)	-0.24(4)	0.41(4)
T(K) 723									
	a (Å)	b (Å)	c (Å)	V/Z (Å ³)					
	7.0073(2)	6.9864(2)	6.9156(1)	84.64					
	x	y	z	U_{iso} or U_{11} (100 Å ²)	U_{22} (100 Å ²)	U_{33} (100 Å ²)	U_{12} (100 Å ²)	U_{13} (100 Å ²)	U_{23} (100 Å ²)
Ga	0	0.1908(3)	$\frac{1}{4}$	2.61(6)					
P	0.3147(5)	0	0	2.02(6)					
O1	0.1935(3)	0.0377(3)	0.1787(2)	4.9(1)	4.4(1)	3.6(1)	2.0(1)	1.2(1)	0.8(1)
O2	0.4377(3)	0.1724(3)	0.9584(3)	5.8(1)	3.8(1)	3.2(1)	-3.1(1)	-0.7(1)	1.0(1)

$5 \times 5 \times 5$ supercell of the β -cristobalite phase of GaPO_4 was refined using RMC modelling of the Bragg profile $F(Q)$ and $D(r)$ data from GaPO_4 at 1303 K. Excellent fits were obtained to all three data sets, comparable to the ones shown in Fig. 6 for the α -quartz phase. The resulting model (see Fig. 11) shows no evidence for either a threefold or sixfold distribution of O atoms between neighboring Ga and P atoms. This is more formally demonstrated by calculating the distribution of the orientation of each tetrahedra with respect to its neighbors in terms of the Ga-O-P angle θ and torsional angle ϕ (the rotation of the P-O bond about the vector defined by the Ga-O bond). This distribution, shown in Fig. 12, has no preferred local orientations and it is concluded that the distribution of O atoms around the vector joining neighboring Ga and P atoms forms a continuous ring broadly centered at $\theta \sim 139^\circ$. Therefore both Rietveld refined average models are (good) approximations of the true O disorder in this phase and nothing can be inferred from the number of partially occupied sites in either average model.

2. α -cristobalite-type structure

Neutron powder diffraction data from α -cristobalite at room temperature and 723 K were refined in space group $C222_1$ without any restraints on any bondlengths or angles. Neither diffraction pattern showed peaks from other phases. The refined structural parameters shown in Table V are consistent with earlier x-ray diffraction work,⁴⁵ although the overall volume expansion is somewhat different, either due to differences in temperature calibration, or resulting from the fact that the neutron data were taken on cooling from the high-temperature β -cristobalite phase.²⁷ The anisotropic adp's for the O atoms imply increased thermal motion perpendicular to the Ga-O and P-O bonds, consistent with rotations of the GaO_4 and PO_4 tetrahedra.

A $5 \times 5 \times 5$ orthorhombic supercell of the α -cristobalite phase of GaPO_4 was refined using RMC modeling of the Bragg profile $F(Q)$ and $G(r)$ data from GaPO_4 at 723 K. Again, excellent fits were obtained to all three data-sets. The resulting model, shown in Fig. 13, retains the local tetrahedral orientations consistent with more limited RUM disorder.

IV. CONCLUSIONS

Total neutron scattering data for gallium phosphate as a function of temperature were used to investigate the progressive increase of thermally induced disorder in the α -quartz-type form and to obtain a better description of the structures of the α - and β -type cristobalite phases. Disorder results in an overestimation of the average structural distortion at high temperature as obtained from Rietveld refinement as can be seen for example in bondlength and bond angle variations, which are in contrast correctly described using RMC refinements of the total scattering data. The deterioration in the piezoelectric properties of the α -quartz form above 1023 K can be correlated to the onset of considerable disorder in the oxygen sublattice, thereby providing a mechanism for the loss of correlation between dipoles. The high-temperature β -cristobalite-type phase was found to be highly disordered. In this cubic structure, the oxygen atoms were found to be distributed in a continuous ring around the Ga-P interatomic vector with a Ga-O-P angle of $\sim 139^\circ$.

ACKNOWLEDGMENTS

The authors are grateful to PIEZOCRYST GMBH for providing high-quality GaPO_4 resonators. This project is supported by a CNRS/Royal Society cooperation agreement.

*Author to whom correspondence should be addressed. Email address: jhaines@lpmc.univ-montp2.fr

¹P. J. Heaney, *Rev. Mineral.* **29**, 1 (1994).

²M. T. Dove, D. A. Keen, A. C. Hannon, and I P Swainson, *Phys. Chem. Miner.* **24**, 311 (1997).

³D. A. Keen and M. T. Dove, *J. Phys.: Condens. Matter* **11**, 9263 (1999).

⁴M. G. Tucker, D. A. Keen, and M. T. Dove, *Miner. Mag.* **65**, 489 (2001).

⁵M. T. Dove, V. Heine, and K. D. Hammonds, *Miner. Mag.* **59**, 629 (1995).

⁶D. M. Hatch, S. Ghose, and J. L. Bjorkstam, *Phys. Chem. Miner.* **21**, 67 (1994).

⁷I. Gregora, N. Magneron, P. Simon, Y. Luspain, N. Raimboux, and E. Philippot, *J. Phys.: Condens. Matter* **15**, 4487 (2003).

⁸J. Haines and O. Cambon, *Z. Kristallogr.* **219**, 314 (2004).

⁹R. A. Young (unpublished).

¹⁰J. Haines, O. Cambon, D. A. Keen, M. G. Tucker, and M. T. Dove, *Appl. Phys. Lett.* **81**, 1 (2002).

¹¹E. Philippot, A. Goiffon, A. Ibanez, and M. Pintard, *J. Solid State*

Chem. **110**, 356 (1994).

¹²E. Philippot, D. Palmier, M. Pintard, and A. Goiffon, *J. Solid State Chem.* **123**, 1 (1996).

¹³E. Philippot, P. Armand, P. Yot, O. Cambon, A. Goiffon, G. J. McIntyre, and P. Bordet, *J. Solid State Chem.* **146**, 114 (1999).

¹⁴J. Haines, C. Chateau, J. M. Léger, and R. Marchand, *Ann. Chim. Sci. Mat.* **26**, 209 (2001).

¹⁵J. Haines, O. Cambon, E. Philippot, L. Chapon, and S. Hull, *J. Solid State Chem.* **166**, 434 (2002).

¹⁶O. Cambon, P. Yot, S. Rul, J. Haines, and E. Philippot, *Solid State Sci.* **5**, 469 (2003).

¹⁷J. Haines, O. Cambon, R. Astier, P. Fertey, and C. Chateau, *Z. Kristallogr.* **219**, 32 (2004).

¹⁸J. Haines, O. Cambon, D. Cachau-Herreillat, G. Fraysse, and F. E. Mallasagne, *Solid State Sci.* **6**, 995 (2004).

¹⁹O. Cambon, J. Haines, G. Fraysse, J. Détaint, B. Capelle, and A. Van der Lee, *J. Appl. Phys.* **97**, 074110 (2005).

²⁰H. Grimm and B. Dorner, *J. Phys. Chem. Solids* **36**, 413 (1975).

²¹K. Kihara, *Eur. J. Mineral.* **2**, 63 (1990).

²²H. Nakae, K. Kihara, M. Okuno, and S. Hirano, *Z. Kristallogr.*

- 210**, 746 (1995).
- ²³E. C. Shafer and R. Roy, *J. Am. Ceram. Soc.* **39**, 330 (1956).
- ²⁴R.-U. Barz, J. Schneider, and P. Gille, *Z. Kristallogr.* **214**, 845 (1999).
- ²⁵K. Jacobs, P. Hofmann, D. Klimm, J. Reichow, and M. Schneider, *J. Solid State Chem.* **149**, 180 (2000).
- ²⁶P. Worsch, B. Koppelhuber-Bitschnau, F. A. Mautner, P. W. Krempf, W. Wallnöfer, P. Doppler, and J. Gautsch, *Mater. Sci. Forum* **312–324**, 914 (2000).
- ²⁷S. N. Achary, O. D. Jayakumar, A. K. Tyagi, and S. K. Kulshrestha, *J. Solid State Chem.* **176**, 37 (2003).
- ²⁸A. C. Hannon, *Nucl. Instrum. Methods Phys. Res. A* **551**, 88 (2005).
- ²⁹A. C. Hannon, W. S. Howells, and A. K. Soper, *Inst. Phys. Conf. Ser.* **107**, 193 (1990).
- ³⁰A. C. Larson and R. B. Von Dreele, *GSAS: General Structure Analysis System*, Los Alamos National Laboratory, Los Alamos, NM, 1994.
- ³¹D. A. Keen, *J. Appl. Crystallogr.* **34**, 172 (2001).
- ³²R. L. McGreevy, *J. Phys.: Condens. Matter* **13**, R877 (2001).
- ³³D. A. Keen, M. G. Tucker, and M. T. Dove, *J. Phys.: Condens. Matter* **17**, S15 (2005).
- ³⁴J. Haines, O. Cambon, and S. Hull, *Z. Kristallogr.* **218**, 193 (2003).
- ³⁵M. S. Ghiorso, I. S. E. Carmichael, and L. K. Moret, *Contrib. Mineral. Petrol.* **68**, 307 (1979).
- ³⁶Y. Maruoka and K. Kihara, *Phys. Chem. Miner.* **24**, 243 (1997).
- ³⁷A. Goiffon, J. C. Jumas, M. Maurin, and E. Philippot, *J. Solid State Chem.* **61**, 384 (1986).
- ³⁸O. Baumgartner, A. Preisinger, P. W. Krempf, and H. Mang, *Z. Kristallogr.* **168**, 83 (1984).
- ³⁹H. Sowa, *Z. Kristallogr.* **209**, 954 (1994).
- ⁴⁰K. Kosten and H. Arnold, *Z. Kristallogr.* **152**, 119 (1980).
- ⁴¹P. Worsch, B. Koppelhuber-Bitschnau, F. A. Mautner, P. W. Krempf, and W. Wallnöfer, *Mater. Sci. Forum* **278–281**, 600 (1998).
- ⁴²A. F. Wright and A. J. Leadbetter, *Philos. Mag.* **31**, 1391 (1975).
- ⁴³H. N. Ng and C. Calvo, *Can. J. Phys.* **55**, 677 (1977).
- ⁴⁴M. G. Tucker, M. P. Squires, M. T. Dove, and D. A. Keen, *J. Phys.: Condens. Matter* **13**, 403 (2001).
- ⁴⁵R. C. L. Mooney, *J. Appl. Crystallogr.* **9**, 728 (1956).
- ⁴⁶D. M. Hatch and S. Ghose, *Phys. Chem. Miner.* **17**, 554 (1991).